SCIENTIFIC REPORTS

OPEN

Control of plasmonic nanoantennas by reversible metal-insulator transition

Received: 08 June 2015
Accepted: 23 July 2015
Published: 11 September 2015

Yohannes Abate[1,2], Robert E. Marvel[3], Jed I. Ziegler[3], Sampath Gamage[2], Mohammad H. Javani[1,2], Mark I. Stockman[1,2] & Richard F. Haglund[3,4]

We demonstrate dynamic reversible switching of VO_2 insulator-to-metal transition (IMT) locally on the scale of 15 nm or less and control of nanoantennas, observed for the first time in the near-field. Using polarization-selective near-field imaging techniques, we simultaneously monitor the IMT in VO_2 and the change of plasmons on gold infrared nanoantennas. Structured nanodomains of the metallic VO_2 locally and reversibly transform infrared plasmonic dipole nanoantennas to monopole nanoantennas. Fundamentally, the IMT in VO_2 can be triggered on femtosecond timescale to allow ultrafast nanoscale control of optical phenomena. These unique features open up promising novel applications in active nanophotonics.

Realizing the potential of nanophotonics for signal and information processing requires control and manipulation of light at subwavelength scales. Optical energy concentration on the nanoscale is achieved on metal nanostructures due to polar electronic modes called surface plasmons (SPs)[1–3]. Photonic crystals are used for complete reflection, guiding, and confinement of light[4], while metamaterials are used to transform light in unconventional ways, making possible such novel devices as perfect absorbers[5] , circular polarizers[6], and selectively reflecting surfaces[7]. While novel devices that control the propagation of light on the nanoscale have been demonstrated[1,8–10], *active* nanoscale control of optical physics in nanostructures is still a major challenge in[11–13], and a bottleneck for, related technologies. Nanoscopic control of the insulator and metallic phases of vanadium dioxide (VO_2) would open up a universe of applications in nanophotonics via modulation of the local dielectric environment of nanophotonic structures, allowing them to function as active device**s.**

In this Article, we demonstrate unprecedented active nanoscale control of concentration of light by single plasmonic infrared antennas in the near-field. The active control of the dielectric environment by the insulator-to-metal transition (IMT) in vanadium oxide (VO_2), dynamically the transforms nanoantennas from dipole to monopole and back. We utilize the local, reversible change of refractive index of VO_2 that undergoes a first-order phase transition from an insulating monoclinic phase to a metallic rutile phase near 70 °C in bulk single crystals[14], the transition can also be induced by strain[15,16] and ultrafast light pulses[17,18]. In polycrystalline VO_2 thin films, the IMT begins as conductive nanodomains nucleate and with increasing temperature evolve to interconnect in a percolative fashion throughout the film[19]. At intermediate stages of the IMT, insulating and metallic phases coexist, forming a network of high- and low-conductivity nanodomains throughout the film. Since the metallic and insulating nanodomains have substantially different refractive indices, VO_2 films provide for direct local control of the dielectric environment at nanometer spatial dimensions, which, in turn, can directly modulate optical responses of nanophotonic structures.

[1]Center for Nano-Optics (CeNO), Georgia State University, Atlanta, Georgia 30303, USA. [2]Department of Physics and Astronomy, Georgia State University, Atlanta, Georgia 30303, USA. [3]Interdisciplinary Materials Science Program, Vanderbilt University, Nashville, TN 37235-1406. [4]Department of Physics and Astronomy, Vanderbilt University, Nashville, TN 37235-1807. Correspondence and requests for materials should be addressed to Y.A. (email: yabate@gsu.edu)

So far, the effects of the VO_2 IMT on plasmonic nanostructures have been studied only in the far-field[20], so that understanding and active control of the near-field interaction by the VO_2 domains has been elusive. Here, we present an experimental study of nanoscale interactions of plasmonic structures with VO_2 undergoing the IMT using scattering-scanning near-field optical microscopy (s-SNOM)[21], which images local vector near-fields with minimal perturbation, indispensable for the study of nanoplasmonic phenomena[22–25]. Image formation in s-SNOM relies on the effective polarizability of tip-sample complex, allowing image contrast that is based on local dielectric environment, which is ideal for nanoscale imaging of IMT.

Results

The model system comprised an array of identical infrared plasmonic nanoantennas: gold nanorods fabricated by e-beam lithography on a 100 nm VO_2 film grown on a $[100]_R$ Si substrate (Fig. 1a). The dimensions of the rods (~2510 nm × 232 nm × 30 nm) were selected to be near-field resonant at mid-infrared frequencies (10.7 μm vacuum wavelength). Near-field optical images were acquired using a commercial s-SNOM system (neaspec.com). A linearly polarized CO_2 laser is focused on the tip–sample interface at an angle of 45° to the sample surface (Fig. 1b). The scattered field is detected by phase-modulation (pseudo-heterodyne) interferometry, yielding topography, amplitude, and phase images[23–26].

First, we investigate the temperature-dependent emergence of metallic nanodomains during the IMT. The temperature was controlled by a heater, and a p-polarized (in the *yz* plane)) excitation laser was tuned to 10.7 μm, with the p-polarized detection (Fig. 1 and Methods). Figure 1 shows the third harmonic (of the tip oscillation frequency) amplitude (A_3) images of VO_2 and the Au nanorod array as a function of temperature. These images reveal the emergence of an anisotropic network of bright domains as the IMT progresses with increasing temperature. While the onset of these local metallic domains appears random, the stripes in fact evolve by connecting to the existing domains in crystallographically preferred directions until a quasi-uniform rutile phase emerges at high temperatures. In the s-SNOM, higher local polarizability in the sample results in stronger near-field optical contrast; hence these near-field images faithfully represent temperature-driven formation of metallic domains in the VO_2 film[19].

The formation of stripe phases was noted soon after the discovery of VO_2. Subsequently, a link was inferred between the stripe phase and substrate strain in high-quality single crystals and thick (250 nm) epitaxial grown by ion-beam assisted sputtering on TiO_2 $[100]_R$ surfaces[27,28]. Stripe formation is also correlated with the power of a near-IR pump laser (1.56 μm), close to the surface-plasmon resonance of the VO_2.

Here, the VO_2 films are thinner (100 nm), polycrystalline, and have no epitaxial relationship to the Si substrate. Nevertheless, the stripe phase appears during the transition from monoclinic to rutile, suggesting that it may occur simply because of localized, in-plane (*xy*) strains that develop at the film surface as individual grains of VO_2 begin to change phase, without any reference to the substrate. This possibility is further supported by the very small height of the stripes seen in the present experiment (Fig. 2).

The IMT metallic stripes appear with localized near-uniform spacing in the near-field amplitude image at an intermediate phase coexistence temperature. These are accompanied by correlated topographic modulation as clearly shown in Fig. 2. Topography (Fig. 2a) and near-field amplitude (Fig. 2b) images are taken at excitation laser wavelength, $\lambda = 10.7\,\mu m$ and temperature, $T = 344\,K$, along with the line profile sketches (Fig. 2c). The topographic variation in our case is smaller (0–3 nm) and the correlation weaker compared to what was observed on a TiO_2 substrate (0–5 nm)[27]. The correlation of the topographic line profile with the periodic stripes is due to a structural change in VO_2 during MIT, which results from the modulation of the rutile and the monoclinic axes.

To directly visualize plasmonic modes of the antennas and their interaction with the IMT of the VO_2 film, we implement in-plane polarization-selective excitation (s-excitation, i.e. polarized along the *y* direction) and in-plane detection (s-detection), which is referred to s/s imaging. Figure 3 shows topography, third-harmonic s/s near-field amplitudes, and phase images of the antennas on the VO_2 film for different temperatures. The four IR antennas are nominally identical (Fig. 3a), making it possible to compare the effects of VO_2 IMT on them. The amplitude images (Fig. 3b–d) show bright and dark optical contrast due to the coexisting insulating (dark) and metallic (bright) phases affecting the nanoscale dielectric environment of the antennas. The metallic phase begins to form randomly with increasing temperature. As a result, portions of the antennas are located partly on the metallic and partly on the insulating phases of VO_2 as observed in the amplitude images (Fig. 3b–d). The amplitude images allow one to see the change of nanoscale field magnitudes and the metallic phase formation. At the same time, the near-field *phase* images Fig. 3e–h) are less sensitive to material contrast but allow one to follow the dipolar mode modification on each of the four antennas due to IMT. They display strong phase contrast at the rod ends. The VO_2 regions exhibit very weak phase contrast as shown in Fig. 3e–h, which is independent of excitation or detection polarizations.

At room temperature, all antennas display identically the expected pronounced dipolar phase contrast at their ends, as shown in Fig. 3e. At higher temperatures, all antennas whose one end is situated on the metallic phase turn from dipole to monopole as evident for Rod 1 (Fig. 3f–h), Rod 3 (Fig. 3f), and Rod 4 (Fig. 3f–g). At even higher temperature, when the amplitude image shows that most of the film is in metallic phase (Fig. 3d), both dipole and monopole antenna modes of Rods 2, 3 and 4 turn off (Fig. 3h) completely. An interesting case is Rod 2: despite the middle part of the rod sitting on the metallic phase

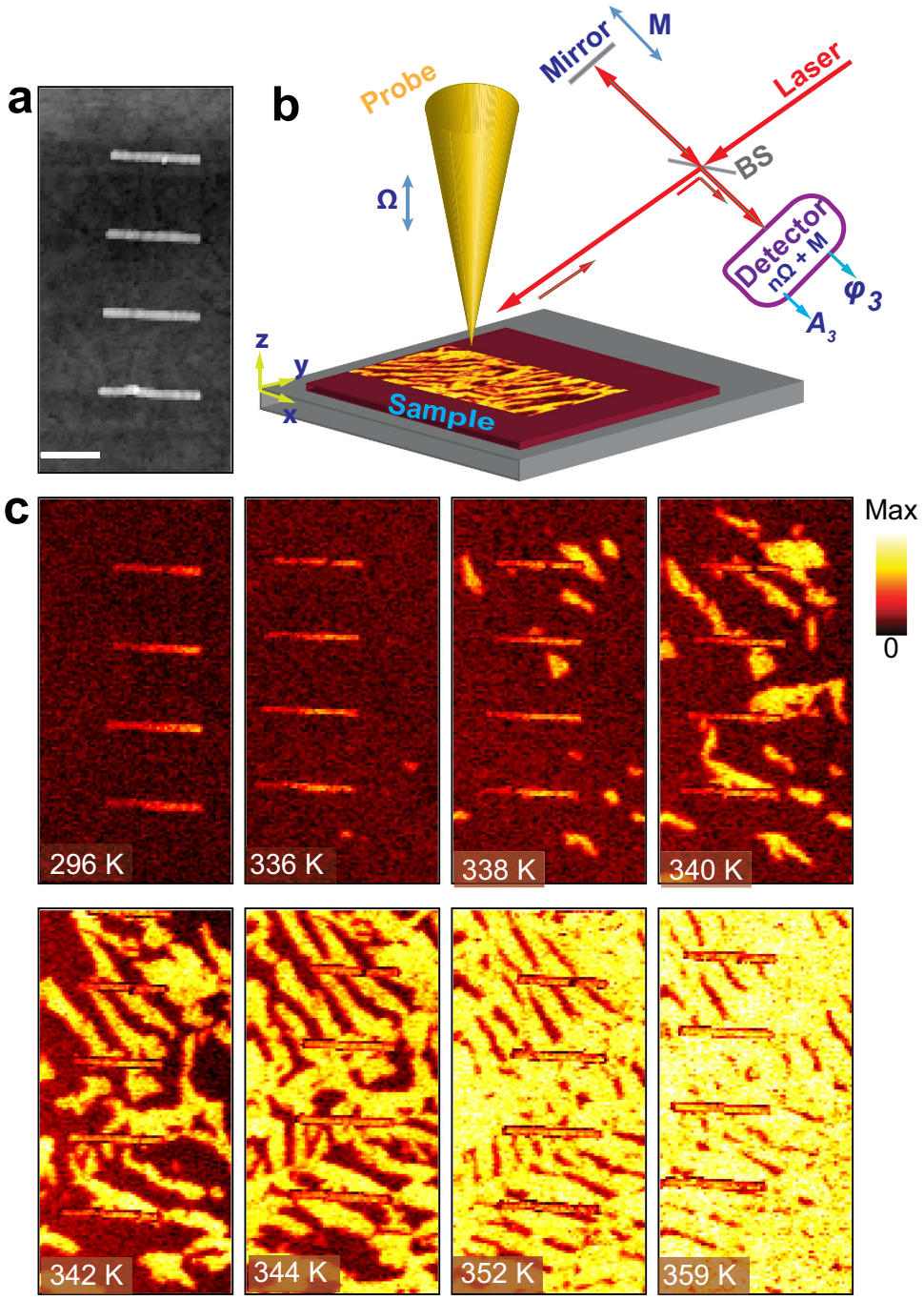

Figure 1. Temperature dependent nanoscale near-field amplitude images of IMT emergence and progress around the infrared antennas. (**a**) Topography of the four antennas on VO_2 film. The scale bar indicates 1 μm. (**b**) Schematic of the s-SNOM experimental setup, which allows polarization-controlled simultaneous imaging of IR plasmonic antenna modes together with the phase spatial evolution of VO_2 phase transition in amplitude and phase. The coordinate system is positioned so that the *y* axis is directed along nanorods and the *z*-axis is normal to the plane of the nanostructure. (**c**) Temperature-dependent near-field amplitude images reveal IMT via forming initial metallic nanodomains, which grow and connect to stripes and quasi-uniform metallic phase.

(Fig. 3c), it still retains its dipole characteristics (Fig. 3g) since both ends are on the insulating grains. It only turns off at higher temperature when the entire antenna is situated on metal (Fig. 3h). These results are interpreted in schematics shown in Fig. 3i–l. This interpretation is supported by numerical calculations performed using the finite difference time-domain (FDTD) simulations (Lumerical Inc.,) shown in Fig. 4, which are in excellent qualitative agreement with experiment.

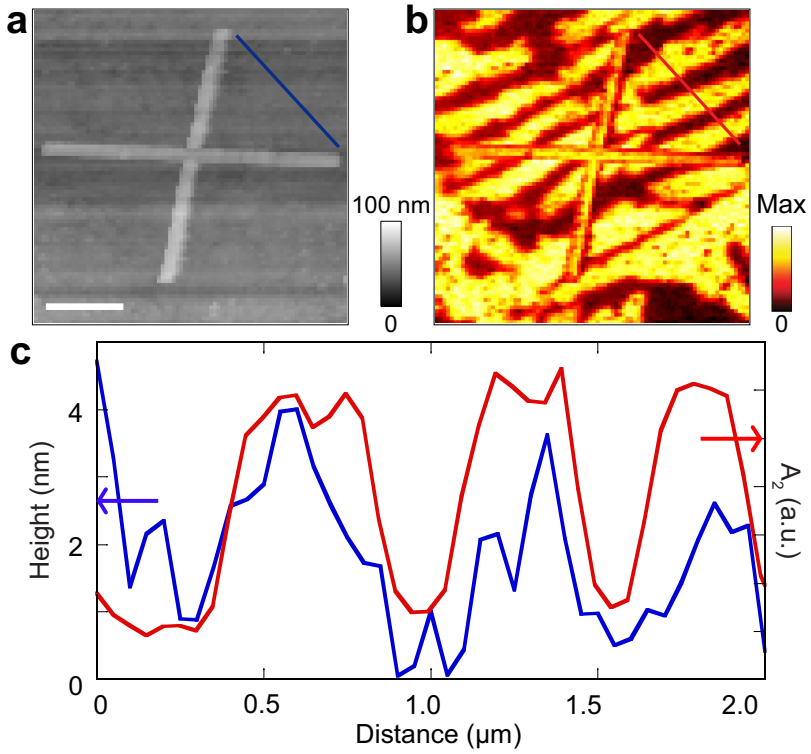

Figure 2. Topography correlation with near-field signal. (**a**) Topography and (**b**) third harmonic near-field amplitude image showing four Au infrared antennas on VO_2 film. (**c**) topography line profile superimposed on amplitude line profile at the marked positions shown by the lines shown in (**a,b**).

Further tracking of active dipole-to-monopole transformation of plasmonic antennas can be performed using s-excitation and p-detection (s/p) cross-polarization selective imaging see Fig. 5. Panel a displays topography, third harmonic optical near-field amplitude and phase images of an Au antenna on the VO_2 substrate at room temperature. The amplitude image displays a stronger optical contrast at rod ends and the phase image shows π phase difference between the rod ends. The amplitude and phase images both exhibit the signature of a dipolar mode of a plasmonic rod expected from S/P cross-polarized excitation/detection experimental method.

Figure 5b shows amplitude contrast of the Au dipolar mode simultaneously with the metallic domain at the onset of phase transition at T = 341 K. Here, the amplitude optical contrast at rod ends is masked by the bright metallic domain contrast of the VO_2 film, and is not clearly distinguishable in the amplitude image. In contrast, the phase image (Fig. 5c) distinctly discriminates the Au plasmonic rod from the metallic background of VO_2 film. As temperature increases (T = 344 K), the metallic phase grows and a portion of one side of the rod sits on the metal and the other side sits on the insulator. The phase image between the rod ends indicates dipole (at T = 296 K and 341 K) to monopole (at T = 344 K) to off (at T = 348 K) transformation of the nanoantenna.

In summary, we have shown the first experimental evidence that *near-field* local optical processes in plasmonic nanostructures can be directly and actively controlled by nanodomains in VO_2 film as it undergoes the IMT. Depending on the precise location of the nanoantennas with respect to metallic and insulating domains in the VO_2 film on the scale of 15 nm or less, the IMT reversibly transforms infrared plasmonic dipole antennas to monopole antennas or switches them off. We envision that such dynamic active control of the nanoscale interaction of light with nanostructured materials, which can potentially be ultrafast, will open up diverse applications in nanooptics and the related technologies.

Methods

Near-field microscopy. The microscope is a commercial s-SNOM system (neaspec.com), which has been described in detail elsewhere. A probing s or p linearly polarized CO_2 laser is focused on the tip–sample interface at an angle of 45° from the sample surface. The scattered field is acquired using a phase modulation, or pseudoheterodyne interferometry. The background signal is suppressed by vertical tip oscillation at the mechanical resonance frequency of the cantilever ($f_0 \sim 285$ kHz) and demodulation of the detector signal at higher harmonics nf_0 (commonly $n = 2, 3$) of the tip resonance frequency. The combined scattered field from the tip and the reference beam pass through a linear polarizer which further selects the p/s polarization of the measured signal for analysis.

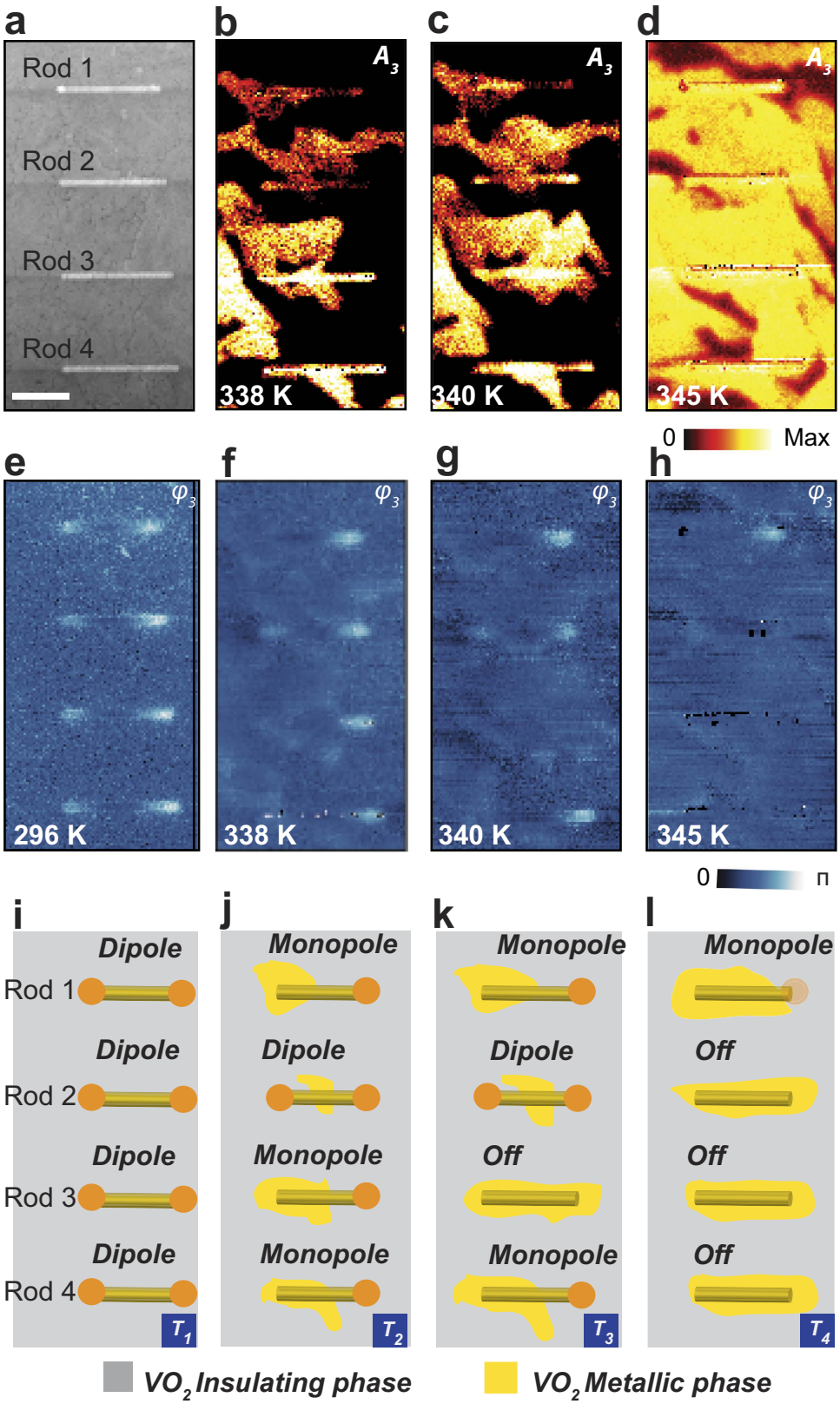

Figure 3. Temperature-controlled IMT and antenna near-field images. Near-field 3rd harmonic amplitude (**b–d**) and phase (**e–h**) images. Schematics (**i–l**) describing experimental results of IR plasmonic antenna modes simultaneously with VO_2 thin film IMT domain formation and propagation.

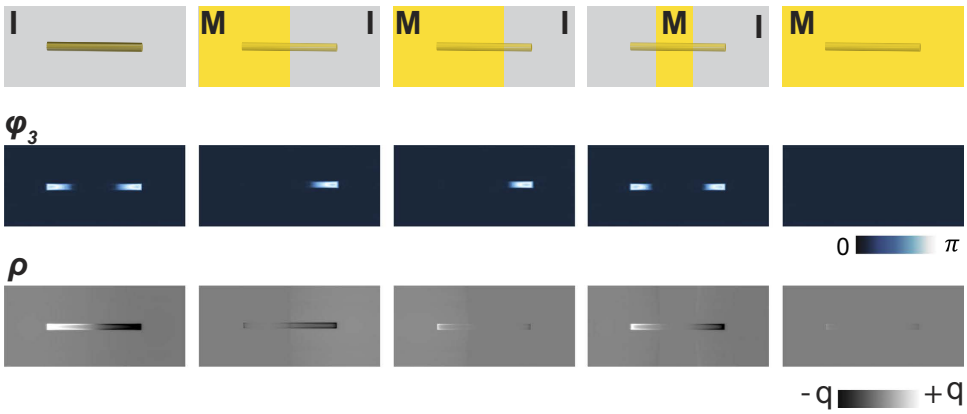

Figure 4. Finite difference time-domain simulations. Single antenna field intensity, phase and surface charge images of FDTD simulations. On schematic of the upper panel, I and M denote insulator and metal phases, respectively.

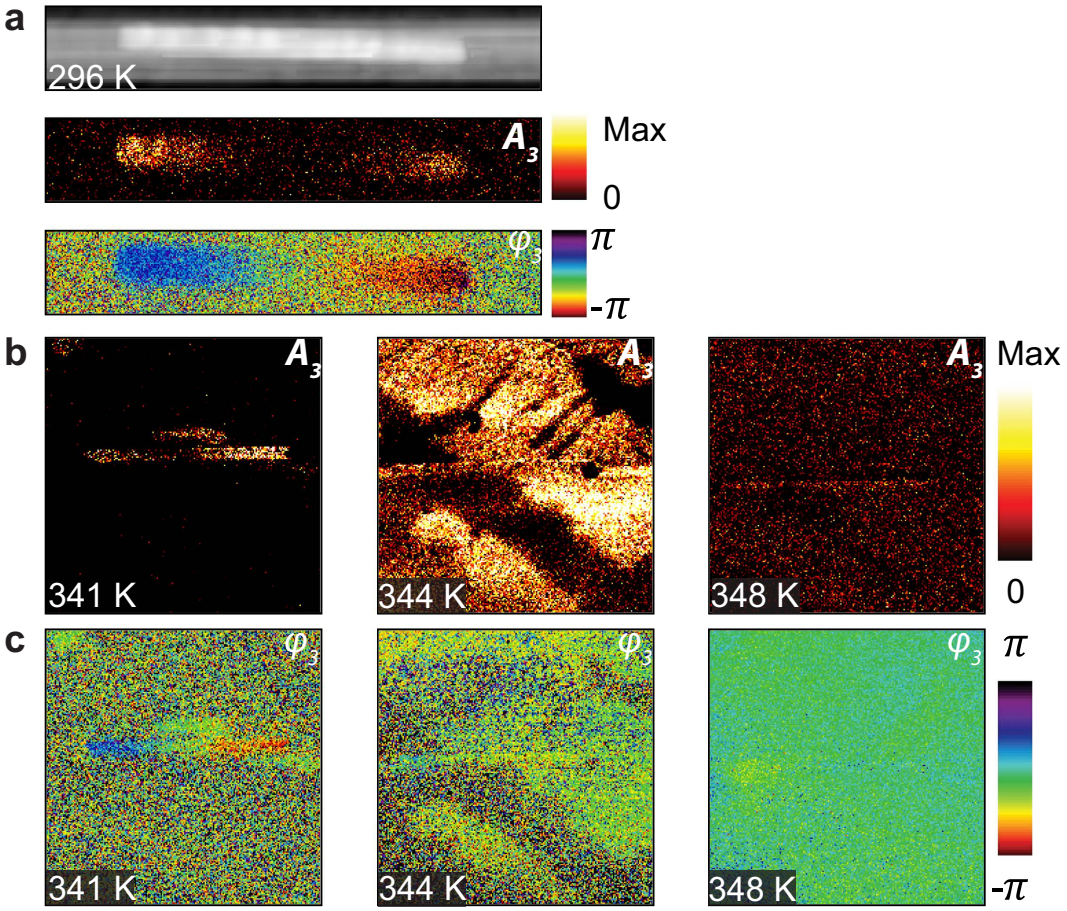

Figure 5. Cross-polarized s/p excitation-detection imaging of plasmons and IMT of VO_2. (**a**) Topography, near-field amplitude and phase images of IR antenna at room temperature. (**b**) near-field amplitude and (**c**) near-field phase images of antenna on VO_2 film at three different temperatures.

Sample fabrication. Amorphous vanadium dioxide films nominally 100 nm thick were deposited on a silicon (100) substrates by electron beam evaporation of a V_2O_4 powder precursor[29]. Annealing at 45 °C in 250 mTorr oxygen crystallized the amorphous films into switching VO_2 with 67 °C phase-transition temperature. A poly(methyl methacrylate) resist (PMMA 495 A4 from Microchem) was spun onto the VO_2 films before fabricating the antenna arrays by electron beam lithography with a Raith eLINE system.

After development of the resist, 50 nm of gold was deposited by thermal evaporation; the remaining resist was removed by lift-off in warm acetone.

Numerical calculations. Experimental results are theoretically interpreted with the aid of finite difference time-domain (FDTD) simulations (Lumerical Inc., lumerical.com). For all simulations each Au rod has dimensions $l = 2512$ nm, $w = 232$ nm and $h = 30$ nm. These dimensions were averaged from topography scan measurements. Each particle is simulated atop a VO_2 substrate. The optical excitation source used for the simulation is a mid infrared (10.7 μm) plane wave. The simulation is performed by assuming a uniform VO_2 film with complex dielectric constant $\varepsilon = 4.9$ for the monoclinic insulating phase and $\varepsilon = -35 + 119i$ for the rutile metallic phase at $\lambda = 10.7$ m[30]. The simulation is performed using both s/s and s/p polarization selective excitation-detection methods.

References

1. Novotny, L. & Hecht, B. *Principles of nano-optics*. (Cambridge University Press, 2012).
2. Maier, S. A. *Plasmonics: fundamentals and applications* (Springer, 2007).
3. Stockman, M. I. Nanoplasmonics: past, present, and glimpse into future. *Opt. Express* 19, 22029–22106, doi: 10.1364/OE.19.022029 (2011).
4. Sievenpiper, D. F., Sickmiller, M. E. & Yablonovitch, E. 3D wire mesh photonic crystals. *Phys. Rev. Lett.* **76,** 2480–2483 (1996).
5. Landy, N. I., Sajuyigbe, S., Mock, J. J., Smith, D. R. & Padilla, W. J. Perfect metamaterial absorber. *Phys. Rev. Lett.* **100,** 207402–207401-207404, doi: 10.1103/Physrevlett.100.207402 (2008).
6. Gansel, J. K. *et al.* Gold Helix Photonic Metamaterial as Broadband Circular Polarizer. *Science* **325,** 1513–1515, doi: 10.1126/science.1177031 (2009).
7. Lin, J. *et al.* Polarization-Controlled Tunable Directional Coupling of Surface Plasmon Polaritons. *Science* **340,** 331–334, doi: 10.1126/science.1233746 (2013).
8. Angelis, F. D. *et al.* Breaking the diffusion limit with super-hydrophobic delivery of molecules to plasmonic nanofocusing SERS structures. *Nature Photonics* **5,** 682–687, doi: 10.1038/NPHOTON.2011.222 (2011).
9. Taminiau, T. H., Stefani, F. D., Segerink, F. B. & Van Hulst, N. F. Optical antennas direct single-molecule emission. *Nature Photonics* **2,** 234–237, doi: 10.1038/nphoton.2008.32 (2008).
10. Giugni, A. *et al.* Hot-electron nanoscopy using adiabatic compression of surface plasmons. *Nat. Nano* **8,** 845–852, doi: 10.1038/nnano.2013.207 http://www.nature.com/nnano/journal/vaop/ncurrent/abs/nnano.2013.207.html - supplementary-information (2013).
11. Krasavin, A. V. & Zheludev, N. I. Active plasmonics: Controlling signals in Au/Ga waveguide using nanoscale structural transformations. *Applied Physics Letters* **84,** 1416–1418 (2004).
12. MacDonald, K. F., Samson, Z. L., Stockman, M. I. & Zheludev, N. I. Ultrafast active plasmonics. *Nature Photonics* **3,** 55–58 (2009).
13. Michel, A. K. U. *et al.* Using Low-Loss Phase-Change Materials for Mid-Infrared Antenna Resonance Tuning. *Nano Letters* **13,** 3470–3475, doi: 10.1021/nl4006194 (2013).
14. Lopez, R., Feldman, L. C. & Haglund, R. F. Size-dependent optical properties of VO_2 nanoparticle arrays. *Physical Review Letters* **93,** doi: 10.1103/PhysRevLett.93.177403 (2004).
15. Cao, J. *et al.* Strain engineering and one-dimensional organization of metal-insulator domains in single-crystal vanadium dioxide beams. *Nature Nanotechnology* **4,** 732–737, doi: Doi 10.1038/Nnano.2009.266 (2009).
16. Park, J. H. *et al.* Measurement of a solid-state triple point at the metal-insulator transition in VO_2. *Nature* **500,** 431–434, doi: 10.1038/nature12425 (2013).
17. Cilento, F. *et al.* Ultrafast insulator-to-metal phase transition as a switch to measure the spectrogram of a supercontinuum light pulse. *Appl. Phys. Lett.* **96,** 0211021–02110213, doi: Artn 021102 Doi 10.1063/1.3291105 (2010).
18. Wegkamp, D. *et al.* Instantaneous Band Gap Collapse in Photoexcited Monoclinic VO_2 due to Photocarrier Doping. *Phys. Rev. Lett.* **113,** doi: Artn 216401 Doi 10.1103/Physrevlett.113.216401 (2014).
19. Qazilbash, M. M. *et al.* Mott transition in VO_2 revealed by infrared spectroscopy and nano-imaging. *Science* **318,** 1750–1753, doi: 10.1126/science.1150124 (2007).
20. Lei, D. Y., Appavoo, K., Sonnefraud, Y., Haglund, R. F. & Maier, S. A. Single-particle plasmon resonance spectroscopy of phase transition in vanadium dioxide. *Opt. Lett.* **35,** 3988–3990, doi: 10.1364/Ol.35.003988 (2010).
21. Keilmann, F. & Hillenbrand, R. Near-field microscopy by elastic light scattering from a tip. *Philosophical Transactions of the Royal Society of London Series a-Mathematical Physical and Engineering Sciences* **362,** 787–805 (2004).
22. Hillenbrand, R. & Keilmann, F. Complex optical constants on a subwavelength scale. *Physical Review Letters* **85,** 3029–3032 (2000).
23. Nuno, Z. *et al.* Nanoscale subsurface- and material-specific identification of single nanoparticles. *Optics Express* **19,** 20865–20875 (2011).
24. Mastel, S. *et al.* Real-space mapping of nanoplasmonic hotspots via optical antenna-gap loading. *Applied Physics Letters* **101,** 131102, doi: 10.1063/1.4754534 (2012).
25. Grefe, S. E. *et al.* Near-field spatial mapping of strongly interacting multiple plasmonic infrared antennas. *Physical Chemistry Chemical Physics* **15,** 18944–18950, doi: 10.1039/C3cp53104j (2013).
26. Stiegler, J. M. *et al.* Nanoscale Infrared Absorption Spectroscopy of Individual Nanoparticles Enabled by Scattering-Type Near-Field Microscopy. *Acs Nano* **5,** 6494–6499, doi: 10.1021/nn2017638 (2011).
27. Liu, M. K. *et al.* Anisotropic Electronic State via Spontaneous Phase Separation in Strained Vanadium Dioxide Films. *Physical Review Letters* **111,** doi: Artn 096602 Doi 10.1103/Physrevlett.111.096602 (2013).
28. Liu, M. K. *et al.* Symmetry breaking and geometric confinement in VO_2: Results from a three-dimensional infrared nano-imaging. *Applied Physics Letters* **104,** doi: 10.1063/1.4869558 (2014).
29. Marvel, R. E., Appavoo, K., Choi, B. K., Nag, J. & Haglund, R. F. Electron-beam deposition of vanadium dioxide thin films. *Applied Physics a-Materials Science & Processing* **111,** 975–981, doi: 10.1007/s00339-012-7324-5 (2013).
30. Qazilbash, M. M. *et al.* Infrared spectroscopy and nano-imaging of the insulator-to-metal transition in vanadium dioxide. *Physical Review B* **79,** doi: 10.1103/PhysRevB.79.075107 (2009).

Acknowledgments

YA acknowledges the major support for this work from DOD (U.S. Army Research Office) Grant No. W911NF-12-1-0076. Work of MIS was supported by Grant No. DE-SC0007043 from the Materials Sciences and Engineering Division of the Office of the Basic Energy Sciences, Office of Science, U.S.

Department of Energy. Fabrication of the VO_2 films by REM was supported by the National Science Foundation (DMR-1207507); e-beam lithography by JIZ was supported by the Office of Science, U. S. Department of Energy (DE-FG02-01ER45916). The samples were fabricated and characterized in facilities funded by the National Science Foundation under the American Recovery and Reinvestment Act (NSF ARI-R2 DMR-0963361).

Author Contributions

Y.A. developed the concept, performed the experiments, analyzed the data and wrote the paper. R.E.M. and J.I.Z. fabricated the sample. S.G. analyzed the data provided support for the experiments. M.H.J. performed the simulations. M.I.S. and R.F.H. developed the concept, provided support for sample fabrication and theoretical calculations, analyzed the data and wrote the manuscript.

Additional Information

Competing financial interests: The authors declare no competing financial interests.

How to cite this article: Abate, Y. *et al.* Control of plasmonic nanoantennas by reversible metal-insulator transition. *Sci. Rep.* **5**, 13997; doi: 10.1038/srep13997 (2015).

This work is licensed under a Creative Commons Attribution 4.0 International License. The images or other third party material in this article are included in the article's Creative Commons license, unless indicated otherwise in the credit line; if the material is not included under the Creative Commons license, users will need to obtain permission from the license holder to reproduce the material. To view a copy of this license, visit http://creativecommons.org/licenses/by/4.0/